

# Combined BEM/FEM vs. 3DFEM Substrate Resistance Modeling

E. Schrik and N.P. van der Meijs

Delft University of Technology, Department of EEMCS, The Netherlands  
e-mail: eelco@cas.et.tudelft.nl

## Abstract

In the context of substrate resistance modeling a combined BEM/FEM method is compared to a 3DFEM method. The combined BEM/FEM method is applicable in substrate modeling problems which involve layout-dependent doping patterns for which a standalone BEM would not be accurate enough and for which a standalone FEM would be too slow. The method captures local couplings within the doping pattern with the FEM, and global couplings through the deep substrate with the BEM. Simulations show that combined BEM/FEM is an appropriate crossover between the BEM and FEM methods. Combined BEM/FEM can be very efficient as the FEM domain is kept small, while a coarse and sparse BEM for the deep substrate is sufficient for accuracy.

## Keywords

substrate modeling, BEM, FEM, combined BEM/FEM

## I. INTRODUCTION

In designing and fabricating present-day micro-electronic circuits, substrate-crosstalk has become an important factor [1]. In order to properly simulate and predict the impact of crosstalk, accurate and efficient substrate modeling methods are very important.

The two main substrate modeling strategies are the boundary discretization methods (like the BEM) and the volume discretization methods (like the FEM). Each of these strategies has its own advantages and disadvantages: the BEM is typically fast, but limited to uniformly layered domains, while the FEM can handle arbitrary domains, but is significantly slower. With substrate structures typically involving layout-dependent doping patterns in the top few microns of the substrate, [2] introduced a combined BEM/FEM method, which handles the doping patterns with the FEM and the deep substrate with the BEM. The resulting hybrid method can be faster than the FEM and more accurate than the BEM.

This paper will show that the combined BEM/FEM method is indeed an appropriate crossover between the BEM and the FEM. We will evaluate the combined BEM/FEM method from [2] against a 3DFEM method, relying on the 3DFEM as an accurate reference method for the studied cases. We will show that the plain 3DBEM fails to match the 3DFEM when the problem involves layout-dependent doping patterns; the errors are unpredictable and can be arbitrarily large. The combined BEM/FEM method, however, shows better behaviour and a much better match with the 3DFEM results, while the computational complexity is typically 1–2 orders of magnitude lower than the 3DFEM.

After a brief introduction of substrate technologies and substrate modeling techniques in Sections II and III, Section IV

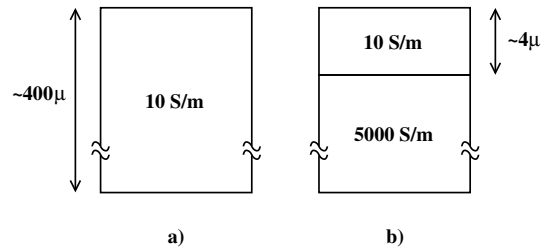


Fig. 1. Typical global doping profiles, a) high-ohmic substrate, b) low ohmic substrate with high-ohmic epi layer on top.

will compare the combined BEM/2DFEM method to a 3DFEM reference through a number of simulations. Section V discusses the simulation results in a wider context and makes suggestions for future work, after which Section VI summarizes and concludes this paper.

## II. SUBSTRATE TECHNOLOGIES

In different types of circuits, different substrate technologies are applied. The behaviour of the substrate w.r.t. crosstalk is mainly determined by two technological influences: the global doping profile and localized doping patterns. Below, we will summarize the most common occurrences of these technological influences based on several sources from literature, in particular [1] and [3]. However, since there are many variations in substrate technologies, the numeric values below should be considered as mere indications.

### A. Global Doping Profiles

In summary, analog and RF IC's typically use a lightly doped substrate (10 S/m, see Figure 1a) because of its low loss, which is beneficial for the quality factor of passive devices. Digital CMOS technologies, however, traditionally use a highly doped substrate (5000 - 10,000 S/m) with a lightly doped epitaxial layer on top (typically several microns thick, with a conductivity of 10 S/m, see Figure 1b). This setup was originally intended to avoid latch-up, but with the lowering of the supply voltage in newer technologies the latch-up problem has been reduced. Thus, in response to the recent increasing number of mixed-signal SoC's, digital and analog technologies are actually converging.

### B. Layout-dependent doping patterns

Apart from the global doping profile, also localized doping patterns may play an important role in crosstalk propagation and/or isolation. These doping patterns are typically present in the top 4 – 6 microns of the substrate, and may be very different depending on the type of circuit. In this paper we will concentrate on the channel-stop layer, being a doping pattern that is commonly used in many circuits.

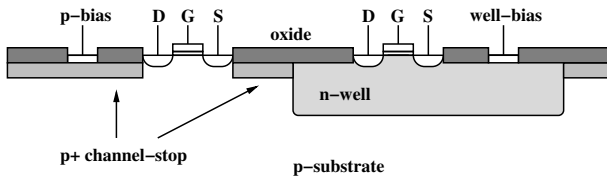


Fig. 2. Schematic representation of common doping patterns in the substrate. The channel-stop layer is interrupted by transistors and wells.

As illustrated in Figure 2, channel-stop is located underneath the oxide (LOCOS, or nowadays STI), to avoid the creation of an inversion layer induced by the lowest levels of the interconnect. In effect, the channel-stop layer raises the threshold voltage of the parasitic FET formed by the lowest levels of interconnect and the underlying substrate. However, since the threshold voltage of the actual transistors should remain as low as possible, the channel-stop layer is not present underneath the transistors themselves. Furthermore, a p+ channel-stop layer does not extend into an n-well (which may have its own n+ channel-stop layer). In other words, the channel-stop layer is a doping pattern which is not present everywhere, but contains holes depending on the layout of the chip. Since the channel-stop layer (typically 1000 S/m) is significantly more conductive than its surroundings (typically 10 S/m), it may either increase or decrease substrate crosstalk between different parts of the chip. As such, including the behaviour of the channel-stopper in a substrate model is important for accuracy.

### III. SUBSTRATE MODELING TECHNIQUES

Substrate resistance extraction involves finding a resistance network between terminals placed on the boundary of a resistive domain. This is a potential-problem known from literature (e.g. [4]), and essentially requires to solve a Laplace equation under appropriate boundary conditions. There are various techniques for finding the solution, as already outlined in [5].

Below, we will briefly summarize the three main modeling techniques used in this paper: the Finite Element Method (FEM), the Boundary Element Method (BEM), and their combination (BEM/FEM).

A fourth technique is the Finite Difference Method (FDM), which can be considered a more restricted version of the FEM. In this paper we only use this technique as an independent reference; it is extensively described in [6].

#### A. Finite Element Method

The finite element method (see e.g. [7]) subdivides the entire domain into triangular (2D) or tetrahedral (3D) elements (see Figure 3a), and treats the elements as linear. The resulting linear relations between the potentials at the corners of the elements (the FEM nodes) can then be expressed by a piecewise linear (or piecewise planar for 3D) function. This linear function implies that every edge in the FEM discretization represents a resistance. In other words, the FEM discretization is equivalent to a resistance network [8]. The resulting network is large and sparse. However, only a small number of the FEM nodes are actually terminal nodes, while the rest of the FEM nodes are internal nodes. Only the terminal nodes are connected to other physical structures (e.g. transistors, vias or possibly a parasitic interconnect capacitance). Therefore, the FEM network will have to be solved such that the internal nodes are eliminated

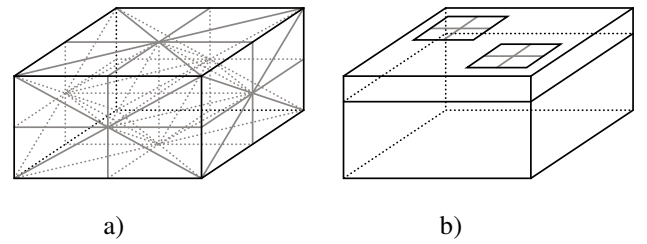


Fig. 3. a) 3D tetrahedral FEM discretization; b) BEM discretization of contact areas on top of uniformly layered domain

and only the resistances between the terminal nodes remain. By writing the FEM network as an admittance matrix (which is also large and sparse), the appropriate solution can be found through Krylov iterative techniques [9] or Gaussian elimination.

The FEM discretization will automatically incorporate any inhomogeneities of the domain into the model, because each element in the discretization has its own material properties assigned. As such, the FEM can be very accurate and flexible.

For substrate modeling problems, the 3DFEM is usually applied. However, when using the BEM/FEM technique (Section III-C), a 2DFEM may sometimes already be sufficient.

#### B. Boundary Element Method

The Boundary Element Method (BEM) is based on an integral form of the Laplace equation [10], [11]

$$\Phi(p) = \int_{S_1} k(q)G(p, q)dq \quad (1)$$

where  $S_1 \subset S$  is the entire contact area on the boundary surface  $S$ ,  $dq$  represents the relevant surface differential,  $k(q)$  represents the unknown continuous current density, and,  $G(p, q)$  is the Green's function.

The Green's function "encodes" the characteristics of the medium, and it can be interpreted physically as "the potential in point  $p$  due to a current injected at point  $q$ ". For the 3D homogeneous case, the Green's function is

$$G(p, q) = \frac{1}{4\pi\sigma r} \quad (2)$$

where  $r = \sqrt{(p_x - q_x)^2 + (p_y - q_y)^2 + (p_z - q_z)^2}$ . Also for uniform, layered media a Green's function can be determined. However, localized doping patterns cannot be included into the Green's function.

The BEM assumes the domain to be a semi-infinite half-space, and only discretizes the contact areas on the top boundary of the domain through which current can enter or leave (see Figure 3b). The discretization usually (but not necessarily) utilizes rectangular panels and assumes a constant current distribution on each panel (i.e. each panel forms an equipotential region), which implements a piecewise constant approximation of the continuous current density distribution. Based on the discretization, the Method of Moments [12] allows to find this approximation from a linear system of equations.

The BEM eventually results in a resistance network. However, compared to a FEM discretization, which is large and sparse, this is a smaller, but *full* resistance network, where each node is a port-node that is connected to every other node. The BEM network can be sparsified by a windowing technique introduced in [10], which also makes the BEM more efficient.

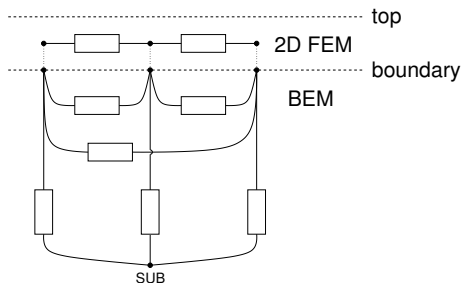


Fig. 4. Side-view of the FEM and BEM domains together with the structure of the resulting resistance models. Due to dual meshing, the nodes on the interface will coincide, and a direct connection between the models can be made.

The BEM network contains one reference node representing the potential at infinity. It is usually referred to as "SUB" or "SUBSTR", see Figure 4, and is inherent in the BEM technique. This reference node provides a sparse representation of global couplings through the deep substrate. Together with the windowing technique, this results in an overall sparser model.

### C. Combined BEM/FEM

When making use of optimized solution methods for both BEM and FEM, the BEM is usually significantly faster. However, for substrate modeling problems which include layout-dependent doping patterns (as in Figure 2), the BEM quickly becomes inaccurate. Even though it is possible to use the FEM in such cases, its limited speed might be prohibitive, especially for larger-scale modeling problems. Therefore, [2] proposed a combined BEM/FEM method which would apply the FEM to the specific doping patterns, and the BEM to the underlying substrate. The BEM and the FEM are then solved as separate problems in their own domains, but which share common variables that are situated on the interface between the domains. The BEM and the FEM both ultimately result in resistance networks, for which the common interface variables correspond to the potentials in the interface nodes. The combined resistance network can then be obtained by making sure that the nodes along the interface are aligned, and attaching the networks through the aligned nodes. This requirement can be met by choosing the BEM mesh as the (Voronoi) dual of the triangular FEM mesh.

Both combined BEM/2DFEM and combined BEM/3DFEM are possible, depending on the characteristics of the FEM domain. In general cases, the 3DFEM can be applied, but in specific cases where the FEM domain is relatively thin, and has a relatively high conductivity compared to the underlying substrate, the resulting field will be predominantly planar and the computationally less expensive 2DFEM can be applied. The resulting networks will then look as illustrated in Figure 4.

## IV. SIMULATIONS

These simulations study the application domain of the BEM/2DFEM method from [2] by comparing it to a full 3DFEM method. The following tools will be used:

- *SPACE* [13]: *Layout-to-circuit extractor with implementations of BEM, 2DFEM and combined BEM/2DFEM.*
- *FEMLAB* [14]: *Multiphysics modeling tool with implementations of 2DFEM and 3DFEM.*
- *RAPHAEL* [15]: *Field solver with implementation of 3DFEM.*

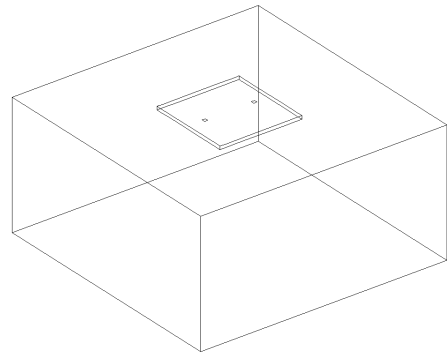


Fig. 5. Example of the simulation setup: a square of channel-stop embedded in a cubic substrate (see Section IV-A).

Both *SPACE* and *FEMLAB* run on the same PIV 2.8GHz machine with 1 Gb of memory. *Raphael* runs on a different machine, but is only used as an independent reference when necessary.

Even though there are fundamental differences between the BEM and the FEM (the BEM assumes the domain to be a semi-infinite half-space, whereas the FEM requires a finite domain), a port-impedance between two terminals on the top boundary of a domain can be calculated by both methods. However, for a proper comparison between the resulting port impedances, the reference node inherent in the BEM technique should be eliminated by Gaussian elimination, and the FEM domain has to be chosen sufficiently large, such that increasing the size of the FEM domain no longer has significant influence on the calculated port impedance. Choosing the FEM domain as a half-cube of  $300 \times 300 \times 150 \mu m$  meets this requirement for the simulations below. An initial simulation with a plain BEM and FEM where the domain was uniformly doped (10 S/m) showed a small difference of 1.86%, while the BEM was an order of magnitude faster and used an order of magnitude less memory than the FEM.

An example of the simulation setup is shown in Figure 5. The FEM domain in the Figure is only  $150 \times 150 \times 75 \mu m$  for easier viewing, but the contacts and square doping pattern (see Section IV-A) have their actual size. The contacts are  $2 \mu m$  by  $2 \mu m$ ,  $30 \mu m$  apart (center-to-center), and are placed flat on the top surface of the domain. The doping pattern is embedded in the domain (i.e. the top planes have the same  $z$  co-ordinate), and may either be square shaped (Section IV-A), or strip shaped (Section IV-B). The doping patterns will have the characteristics of a channel-stop layer: we choose the typical thickness to be 0.5 micron and the typical conductivity to be 1000 S/m. The last simulation (Section IV-C) studies a realistic channel-stop pattern from a ring-oscillator design.

The applicability of the BEM/2DFEM method will be studied by performing a set of simulations under varying thickness and by performing a second set of simulations under varying conductivities. The thickness range under investigation will be from  $0.25$  to  $16 \mu m$ . Even though a doping pattern as thick as  $16 \mu m$  is unlikely, we have included it in the simulation because the dimensions can be scaled, giving insight into the case of constant thickness, but reduced contact dimensions. The conductivity range will be from 10 S/m (typical bulk conductivity) to 10,000 S/m (typical buried-layer conductivity), at a fixed layer thickness of  $2 \mu m$ .

TABLE I  
EXTRACTION STATISTICS FOR SQUARE ( $0.5 \mu\text{m}$  THICK,  $1000 \text{ S/M}$ ).

	3DFEM	BEM/2DFEM	
	(reference)	fine	coarse
memory (Mb)	600	32.9	2.86
time (s)	780	2.5	0.8
resistance ( $k\Omega$ )	2.112	1.886	1.784
relative error (%)	0	-10.7	-15.5

### A. Square structure

The following simulations will be performed on the square structure as shown in Figure 5. The square is  $50 \times 50$  microns in size.

#### Verification of Accuracy

In this simulation, we study the accuracy behaviour of the BEM/2DFEM method with a coarse mesh on the BEM/FEM interface ( $10 \times 10$  grid; 100 interface contacts), and with a fine mesh ( $25 \times 25$  grid; 625 interface contacts).

The extraction statistics for these extractions are displayed in Table I, where they are compared to the 3DFEM. While the accurate extraction differs from the 3DFEM result by some 11%, it is 2 orders of magnitude faster and uses an order of magnitude less memory than the 3DFEM.

#### Influence of BEM window size and BEM discretization

In the simulations from Table I, we used a small BEM window of  $5 \mu\text{m}$ . Increasing the window size makes the extraction computationally more expensive, but the calculated value remains approximately the same, as Table II indicates<sup>1</sup>. Only at a very small window size the result starts to decrease.

The fact that the BEM window has little influence on the final result confirms that the FEM takes into account the local couplings, while the BEM takes into account the global couplings (mainly through the reference node representing the potential at infinity).

Furthermore, Table I was generated with the grid of interface contacts (625 contacts in the fine extraction) having only 1 BEM element on each contact. Increasing the number of BEM elements per contact (i.e. applying mesh refinement to the BEM mesh), we obtain the results from Table III. Here, we observe that refining the BEM mesh has only marginal influence on the resulting resistance value.

From these observations, we conclude that the interface discretization is the most important factor in the convergence of the BEM/2DFEM method, while the BEM window and the BEM discretization have only small, second order effects on the final result. This implies that a BEM extraction with a relatively coarse mesh and a small window is sufficient for the combined BEM/2DFEM results to be accurate. Thus, the BEM extraction can be chosen such that it contributes only little to the computational complexity of the overall combined BEM/2DFEM extraction, while appropriate accuracy is still achieved.

<sup>1</sup>The resistance and memory values for increasing window size do not change monotonically due to meshing artefacts induced by the window, but the overall trend is still visible.

TABLE II  
EXTRACTION STATISTICS FOR VARYING BEM WINDOW SIZE IN THE FINE BEM/2DFEM EXTRACTION (625 INTERFACE CONTACTS) OF THE SQUARE STRUCTURE ( $0.5 \mu\text{m}$  THICK,  $1000 \text{ S/M}$ ).

window size ( $\mu\text{m}$ )	time (s)	memory (Mb)	$R_{AB}(k\Omega)$
2	0.85	24.9	1.799
5	2.5	32.9	1.886
10	4.1	26.3	1.911
20	18.0	32.0	1.896
50 (full)	30.0	60.2	1.889

TABLE III  
EXTRACTION STATISTICS FOR INCREASING BEM DISCRETIZATION UNDER FIXED BEM WINDOW SIZE ( $10 \mu\text{m}$ ) IN THE FINE BEM/2DFEM EXTRACTION (625 INTERFACE CONTACTS) OF THE SQUARE STRUCTURE ( $0.5 \mu\text{m}$  THICK,  $1000 \text{ S/M}$ ).

av. #elem/contact	time(s)	mem(Mb)	$R_{AB}(k\Omega)$
1	4.1	26.3	1.911
2	5.2	26.7	1.903
4	7.9	29.1	1.891
8	29.3	39.4	1.881
16	211	75.5	1.869

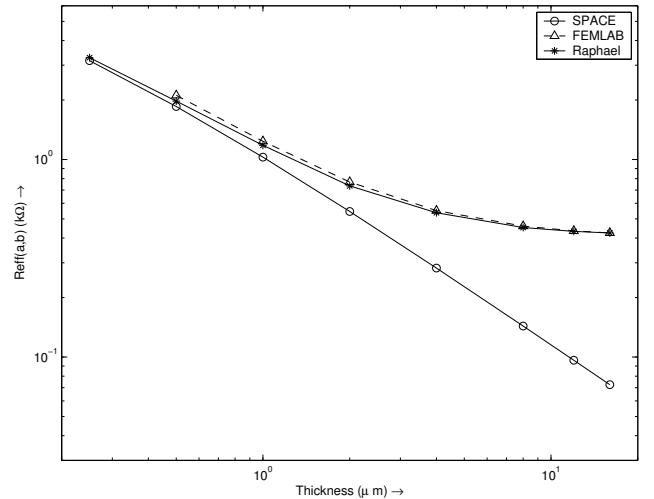


Fig. 6. Square: varying channel-stop thickness at  $1000 \text{ S/m}$  conductivity

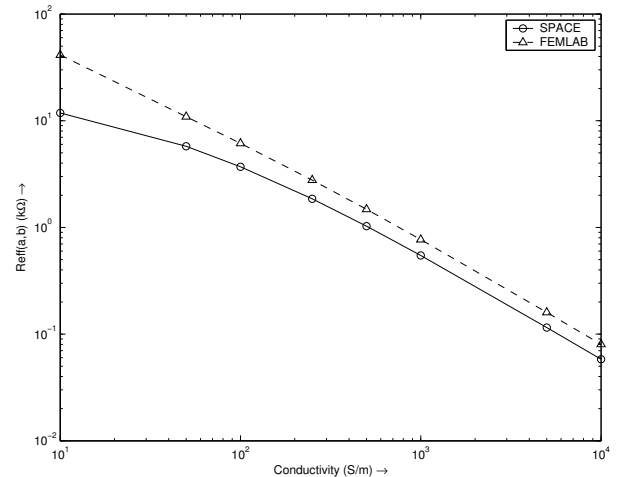


Fig. 7. Square: varying channel-stop conductivity at  $2 \mu\text{m}$  thickness

TABLE IV  
EXTRACTION STATISTICS FOR STRIP (0.5  $\mu\text{m}$  THICK, 1000 S/M).

	3DFEM (reference)	BEM/2DFEM	
		fine	coarse
memory (Mb)	210	0.617	0.363
time (s)	120	0.0	0.0
resistance ( $k\Omega$ )	11.91	13.42	12.87
relative error (%)	0	+12.7	+8.06

#### Influence of domain thickness and conductivity

Figures 6 and 7 show the simulations for varying thickness and varying conductivity of the channel-stop layer.

We observe that the behaviour of the BEM/2DFEM method is not very robust for this situation. The thickness simulations show that the method performs well for a channel-stop layer with a thickness of up to approximately 1  $\mu\text{m}$ . The conductivity simulations show that the method converges to a constant error of around 25–30 % for the layer of 2  $\mu\text{m}$  thickness.

#### Explanation of the errors

The errors in the results above are primarily caused by the fact that the 2DFEM cannot include any vertical components in the field, which become apparent for thicker, and lower-conductivity doping patterns. A 3DFEM is expected to achieve much better accuracy in such cases. For example, if we use the SPACE 2DFEM, FEMLAB 2DFEM and FEMLAB 3DFEM to model just the square channel-stop area at various thicknesses, we obtain:

	FEMLAB		SPACE
	3DFEM	2DFEM	2DFEM
0.5 $\mu\text{m}$	2.58	2.44	2.39
1 $\mu\text{m}$	1.37	1.22	1.20
2 $\mu\text{m}$	0.807	0.611	0.597

We observe that the 2DFEM methods in SPACE and FEMLAB support each other very well, but that the 2D and 3D FEM methods support each other only for thin structures. Apparently, the square structure is a difficult case in the sense that it quickly renders the 2DFEM inaccurate as the structure becomes thicker.

#### B. Strip structure

The strip structure utilizes the same domain as in Figure 5, but the square pattern has been replaced with a strip of 32x2 microns, which connects the two terminals on top. For the strip structure we have verified accuracy and have done thickness/conductivity simulations over the same parameter range as for the square structure.

Table IV shows the extraction statistics for the accuracy verification. The BEM window is now 10  $\mu\text{m}$ , but a full window still results in negligible extraction times. We observe that the fine extraction with the BEM/2DFEM method results in a larger error than the coarse extraction. Even though the error can partly be reduced by choosing a finer BEM discretization (cf. Table III), the BEM/2DFEM method apparently converges to an overestimation of the resistance. This is probably caused by the current implementation of the BEM/2DFEM method which does not model the sidewall of the strip implant. This observation is confirmed by a FEMLAB simulation with the sidewall effects

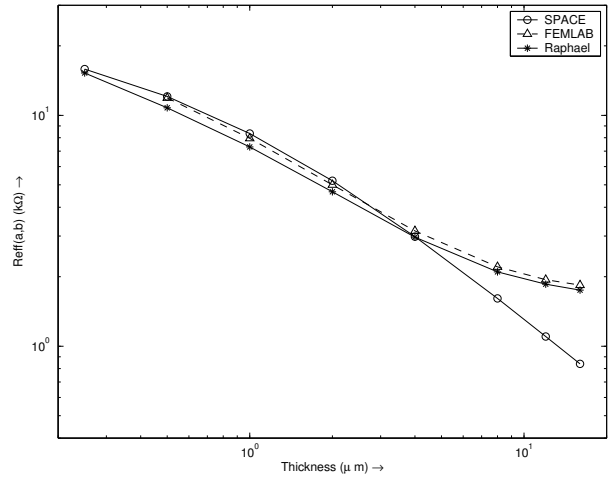


Fig. 8. Strip: varying channel-stop thickness at 1000 S/m conductivity

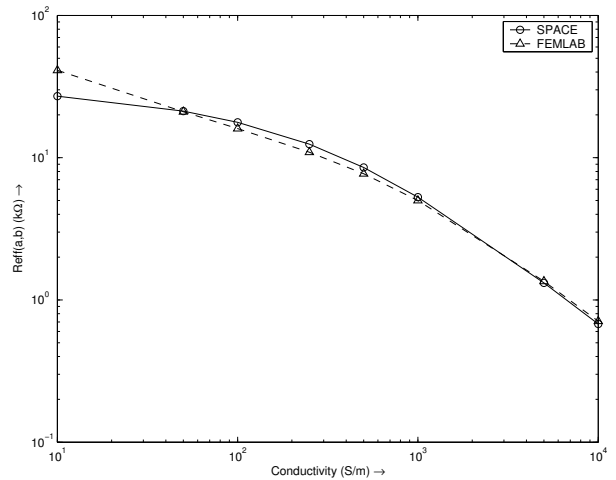


Fig. 9. Strip: varying channel-stop conductivity at 2  $\mu\text{m}$  thickness

omitted, which finds  $R_{AB} = 13.53k\Omega$ .

Despite the difference in modeling approach, the thickness and conductivity simulations in Figures 8 and 9 show good behaviour. The combined BEM/2DFEM still yields acceptable results for thicker structures. This seems to contradict the observation from the previous paragraph, but as the pattern gets thicker, the resistance of the structure will become lower, which concentrates the current inside the structure. The amount of current through the sidewall then becomes less significant.

#### C. Ring oscillator

This simulation continues on previous work from [16], where the substrate noise generated by a 9-section ring-oscillator (see Figure 10) was studied, and the individual noise contributions from the various noise sources (transistors and interconnect) were identified.

Here, we will use the same ring oscillator (250 nm gate length, 10 S/m substrate) but we will now also model the channel-stop pattern as in Figure 11. Note the empty areas in the channel-stop pattern, which originate from the transistors and the n-well. In larger designs, the n-wells may cover significant areas, which renders a BEM approach with a layered Green's function (see Section III-B) inaccurate.

Figure 12 shows the simulation results for the noise wave-

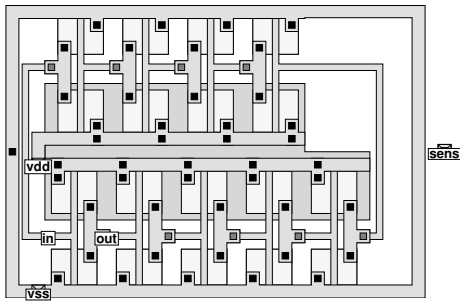


Fig. 10. 9-section ring oscillator

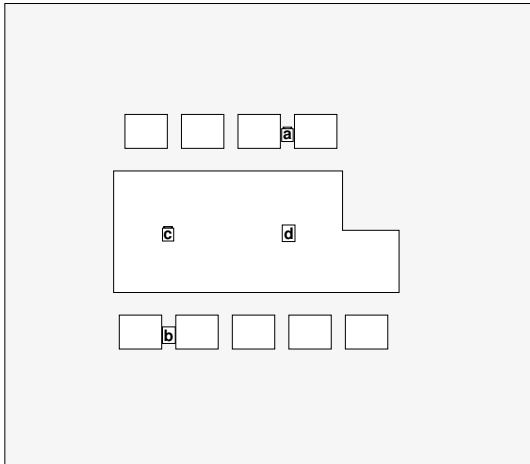


Fig. 11. Channel-stop pattern for the ring oscillator. Markers are test-terminals for the simulations in Table V.

forms on the sensor node (just outside the right-hand edge of the oscillator, See Figure 10). The presence of the channel-stop layer has a significant impact on the shape of the waveforms, and causes the waveform to keep much closer to zero, except for the periodic high peaks. Choosing a channel-stop layer of 1 micron thick, the waveform changes only slightly.

With the channel-stop layer included, the oscillation frequency in the simulation is 876 MHz, whereas without the channel-stop layer, this is slightly lower at 870 MHz.

#### BEM vs. BEM/2DFEM vs. 3DFEM

FEMLAB is not capable of doing circuit simulations. However, choosing different configurations of test terminals in the channel-stop pattern (see Figure 11) and calculating the resistance between them with the various methods, gives at least an indication of the accuracy of the results.

Table V shows the numerical values of the comparison. Columns  $R_{ab}$  and  $R_{cd}$  have been generated by separately simulating with terminal configurations  $ab$  and  $cd$  from Figure 11. In terminal configuration  $ab$ , both terminals have been placed on top of the channel-stop layer, whereas in terminal configuration  $cd$ , both terminals have been placed on locations where no channel-stop is present.

In column  $R_{ab}$ , we observe that 3DFEM, combined BEM/2DFEM and double-layer BEM are near each other, whereas the single-layer BEM gives a large error. However, in column  $R_{cd}$  we observe that 3DFEM, combined BEM/2DFEM and single-layer BEM are near each other, whereas the double-layer BEM gives a large error. This confirms that the behaviour of BEM/2DFEM is similar to the 3DFEM, whereas either the

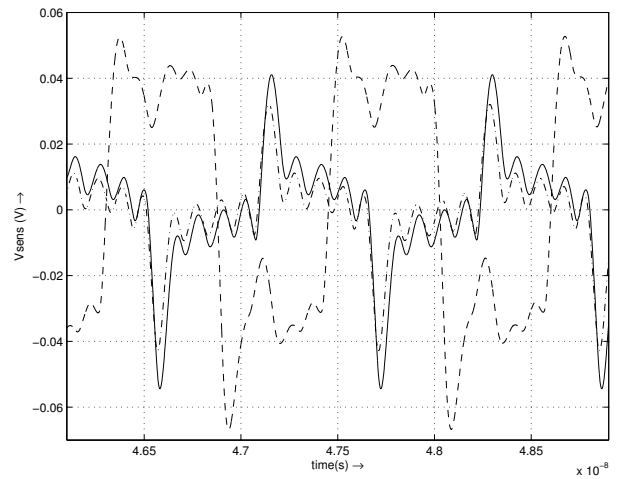


Fig. 12. Simulated noise waveform on the sensor node outside the ring oscillator, with channel-stop of  $0.5\mu\text{m}$  thick (solid),  $1\mu\text{m}$  thick (dash-dot) and without channel-stop (dashed).

TABLE V

RESISTANCE VALUES FOR THE VARIOUS MODELING APPROACHES WITH THE DIFFERENT WAYS OF HANDLING CHANNEL-STOP.  $R_{ab}$  AND  $R_{cd}$  CALCULATED BETWEEN THE TWO CORRESPONDING MARKERS IN FIGURE 11. CHANNEL-STOP CONDUCTIVITY 1000 S/M, THICKNESS  $0.5\mu\text{m}$ .

method	channel-stop	$R_{ab}$ ( $k\Omega$ )	$R_{cd}$ ( $k\Omega$ )
1-layer BEM	absent	231.4	227.2
3DFEM	pattern	7.270	213.6
BEM/2DFEM	pattern	5.802	245.3
2-layer BEM	uniform layer	3.606	3.281

single-layer or the double-layer BEM can give very large errors, depending on the situation.

From Figure 12 it is clear that there is only a marginal difference in the waveforms when choosing a  $1\mu\text{m}$  thick channel-stop pattern instead of a  $0.5\mu\text{m}$  thick channel-stop pattern. Apparently, the general topology and consistency of the model already determine the accuracy of the simulations, rather than the highest accuracy in the resistance values. Therefore, considering the appropriate match between the 3DFEM and the combined BEM/2DFEM method in Table V, it is expected that the BEM/2DFEM model is sufficient for accurate simulations.

#### V. DISCUSSION

In the previous simulations, we observed that the combined BEM/2DFEM method might, or might not, be accurate enough depending on the modeling requirements, technological parameters and the geometry of the doping pattern.

In cases where BEM/2DFEM does not reach sufficient accuracy, we could use a BEM/3DFEM method. Our current research aims at developing such a method. Figure 13 illustrates the approach<sup>2</sup>. We foresee that the 3DFEM allows a reduced-order approach which can be achieved by observing that any vertical components in the field are most significant near the contact areas, whereas the field will be mainly horizontally oriented at some distance from the contacts. In the areas where the field is horizontally oriented, the vertical field component will

<sup>2</sup>It could be argued that the 3DFEM segment as shown in Figure 13 resembles a 3DFEM, but conceptually this makes no difference since the FDM is actually a restricted FEM.

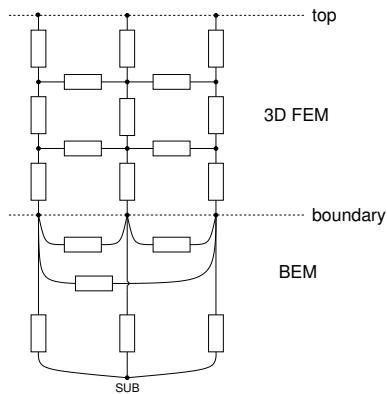


Fig. 13. Combined BEM / 3DFEM.

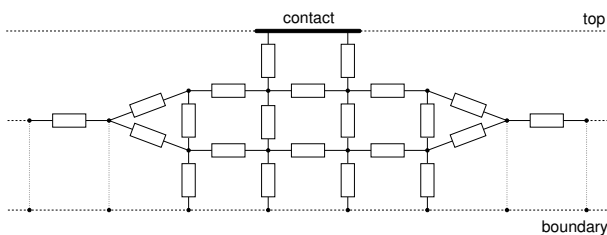


Fig. 14. 3DFEM around contact areas, node contraction at longer distances.

be negligible, causing the nodes in the vertical discretization to be almost equipotential. If these nodes are properly aligned, which we could ensure by generating the 3DFEM discretization in a specific way, they can be contracted. In other words, stacked equipotential nodes can be contracted into a single node without introducing any error (conceptually equivalent to [17]). This allows to use the 2DFEM in these areas; the principle is indicated in Figure 14. The result would be a mixed 2D/3DFEM approach, which we can combine with the BEM as before.

Even though we did not yet do any simulations, we expect that a coarse BEM still provides sufficient accuracy in a combined BEM/3DFEM extraction (either with or without node contractions). In terms of the system of equations that describes our modeling problem, this means that the sparse 3DFEM system for the local effects is supplemented with a sparse BEM system for the global effects. Together, this forms a sparse system of equations, which we currently solve with a solver based on Gaussian elimination. Using this solver, the combined BEM/FEM method compares favorably to the 3D methods from FEMLAB and RAPHAEL. However, the system of equations might be solved with a faster iterative solver [9], as would typically be used in dedicated substrate modeling tools like the 3DFDM tool SubstrateStorm [18].

Thus, we expect that BEM/3DFEM can be as accurate as a full 3DFDM or 3DFEM, while it would use fewer variables and would retain sparsity. In particular, the 3DFDM discretizes the substrate into several layers of cuboids. In order to take the thickness of the substrate properly into account, the 3DFDM also has to define discretization layers in the deep substrate. Conceptually, our BEM/3DFEM method could use the same discretization in the top layers, but it requires no discretization layers in the deep substrate, because that is handled by the (coarse) BEM. Our overall system of equations is then inherently smaller and retains sparsity.

## VI. CONCLUSIONS

We have shown that the combined BEM/FEM method is an appropriate crossover between the BEM and FEM methods. Where a standalone FEM typically generates a large and sparse model, the combined method only applies the FEM to smaller subdomains. This keeps the size of the FEM network as small as possible, while retaining the sparsity. Furthermore, simulations show that the accuracy of the combined model does not depend strongly on the extraction settings of the BEM: a small window and a coarse mesh are sufficient. The resulting BEM network is sparse. The overall combined model is then small and sparse, while accuracy is still ensured. As such, the combined method inherits good characteristics from both its constituting parts.

We have made preliminary suggestions for a reduced-order 3DFEM, which contracts equipotential nodes in the 3DFEM network. Future work will investigate this new method further.

## REFERENCES

- [1] S. Donnay and G. Gielen (Eds.). *Substrate Noise Coupling in Mixed-Signal ASICs*. Kluwer Academic Publishers, 2003.
- [2] E. Schrik and N.P. van der Meijs. Combined bem/fem substrate resistance modeling. In *Proc. 39th DAC*, pages 771–776, 2002.
- [3] J.L. González X. Aragonès and A. Rubio. *Analysis and Solutions for Switching Noise Coupling in Mixed-Signal ICs*. Kluwer, 1999.
- [4] E. Weber. *Electromagnetic Fields, Theory and Applications – Volume 1, Mapping of Fields*. Wiley, 1950.
- [5] E. Schrik, P.M. Dewilde, and N.P. van der Meijs. Theoretical and practical validation of combined bem/fem substrate resistance modeling. In *Proc. ICCAD*, pages 10–15, 2002.
- [6] A.R. Mitchell and D.F. Griffiths. *The Finite Difference Method in Partial Differential Equations*. Wiley, 1994.
- [7] P.P. Silvester and R.L. Ferrari. *Finite Elements for Electrical Engineers*. Cambridge University Press, 1996, 3rd ed., 1996.
- [8] A.J. van Genderen. *Reduced Models for the Behavior of VLSI Circuits*. PhD thesis, Delft University of Technology, 1991.
- [9] Y. Saad. *Iterative Methods for Sparse Linear Systems*. 2nd ed., Philadelphia : Society for Industrial and Applied Mathematics, 2003.
- [10] T. Smedes, N.P. van der Meijs, and A.J. van Genderen. Extraction of circuit models for substrate cross-talk. In *Proc. ICCAD*, pages 199–206, 1995.
- [11] C.A. Brebbia. *The Boundary Element Method for Engineers*. Pentech Press, 1978.
- [12] R.F. Harrington. *Field Computation by Moment Methods*. Krieger, reprint edition 1982 (1968).
- [13] F. Beefink, A.J. van Genderen, N.P. van der Meijs, and J. Poltz. Deep-submicron ulsi parasitics extraction using space. In *Proc. DATE, Designer Track*, pages 81–86, 1998.
- [14] *FEMLAB: Multiphysics Modeling Based on Finite Element Technology*, [www.comsol.com](http://www.comsol.com).
- [15] *Raphael: Field Solver with FDM and BEM support, part of the Taurus environment by Synopsys*, [www.synopsys.com](http://www.synopsys.com).
- [16] E. Schrik, A.J. van Genderen, and N.P. van der Meijs. Coherent interconnect/substrate modeling using space - an experimental study. In *Proc. 33rd ESSDERC*, pages 585–588, 2003.
- [17] A.J. van Genderen and N.P. van der Meijs. Using articulation nodes to improve the efficiency of finite-element based resistance extraction. In *Proc. 33rd DAC*, pages 758–763, 1996.
- [18] *SubstrateStorm: dedicated substrate modeling tool, part of the Cadence design environment*, [www.cadence.com](http://www.cadence.com).